Edge State, Band Topology, and Time Boundary Effect in the Fine-Grained Categorization of Chern Insulators

H. C. Wu,[1,2] H. S. Xu,[1] L. C. Xie,[1] and L. Jin[1,*]
[1]School of Physics, Nankai University, Tianjin 300071, China
[2]School of Physics, Zhengzhou University, Zhengzhou 450001, China

(Received 24 July 2023; accepted 10 January 2024; published 22 February 2024)

We predict novel topological phases with broken time-reversal symmetry supporting the coexistence of opposite chiral edge states, which are fundamentally different from the photonic spin-Hall, valley-Hall, and higher-order topological phases. We find a fine-grained categorization of Chern insulators, their band topologies characterized by identical Chern numbers are completely different. Furthermore, we prove that different topologies cause zeros in their Bloch wave function overlaps, which imprint the band gap closing and appear at the degenerate points of topological phase transition. The Bloch wave function overlaps predict the reflection and refraction at a topological time boundary, and the overlap zeros ensure the existence of vanishing revival amplitude at critical times even though different topologies before and after the time boundary have identical Chern numbers. Our findings create new opportunities for topological metamaterials, uncover the topological feature hidden in the time boundary effect as a probe of topology, and open a venue for the exploration of the rich physics originating from the long-range couplings.

DOI: 10.1103/PhysRevLett.132.083801

Topological phases of matter have nontrivial band structures and support topological states robust against disorder at the edges and interfaces of photonic topological systems [1–13]. Topological invariants characterize the topology of Bloch bands and predict the number of topological edge and interface states, known as the bulk-boundary correspondence [14–17]. This is a fundamental principle and explains why the detection of topological invariants is important in topological physics [18–23]. For two-dimensional topological phases, the Chern number as a topological invariant predicts the number of chiral edge states in the photonic topological insulators created from breaking the time-reversal symmetry [24–31]. Furthermore, the time-reversal symmetric insulating phases may have nontrivial topology although they have a zero Chern number. For example, the photonic spin-Hall phase created from breaking the time-reversal symmetry of each individual pseudospin is characterized by the opposite nonzero spin-Chern numbers [32–43], which predict the numbers of chiral edge states associated with the pseudo-spin-up and pseudo-spin-down. The valley is another degree of freedom similar to the spin, but the photonic valley-Hall phase is created from breaking the inversion symmetry [44–52]. In addition, the time-reversal symmetric quadrupole topological phase also has a zero Chern number [53–62]. This nontrivial higher-order topology supports the corner states. Clearly, the time-reversal symmetry preserving topological insulating phases have completely different topologies. A question naturally arises: do novel time-reversal symmetry breaking topological insulating phases exist with unveiled band topologies? If yes, how does one characterize and probe such topological phases?

In this Letter, we predict novel Chern insulators simultaneously holding the opposite chiral edge states with broken time-reversal symmetry, which fundamentally differs from the photonic spin-Hall, valley-Hall, and higher-order topological phases. We find a fine-grained categorization of Chern insulators. The positive and negative charges of Berry connection singularities (BCSs) distinguish the topological phases and predict the numbers of clockwise and counterclockwise chiral edge states, respectively. We further find that different topologies cause zeros in their Bloch wave function overlaps, which predict the time reflection and refraction at a photonic time boundary. We propose the time boundary effect as a probe of topology. The time boundary effect is the temporal analogy of the spatial boundary effect based on the space-time duality. The vanishing of time reflection or refraction imprints the band gap closing in the topological phase transitions and ensures the existence of vanishing revival amplitude at critical times when the systems before and after the time boundary have different topologies even though their Chern numbers are identical. The coexistence of opposite chiral edge states with different velocities create new opportunities for the development of robust photonic devices. The discovery of the fine-grained

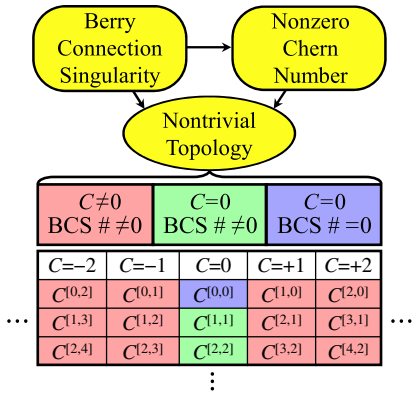

FIG. 1. Topological phases characterized by the BCSs. The BCS and nonzero Chern number cause nontrivial topology. The nonzero Chern number is attributed to the BCS. The presence of BCS may cause nontrivial topology with a nonzero Chern number (in red) or a zero Chern number (in green). The absence of BCS can have nontrivial topology (in purple). See Supplemental Material A for examples [63].

categorization of Chern insulators provides profound insight into the bulk-boundary correspondence for the novel two-dimensional topological phases of matter. The time boundary effect offers a promising platform for the detection of topology.

We consider a two-band Bloch Hamiltonian $H(\mathbf{k}) = \mathbf{B}(\mathbf{k}) \cdot \sigma + B_0(\mathbf{k})\sigma_0$, where $\mathbf{B}(\mathbf{k}) = [h_x(\mathbf{k}), h_y(\mathbf{k}), h_z(\mathbf{k})]$ is an effective magnetic field, $\mathbf{k}$ is the momentum, $\sigma = (\sigma_x, \sigma_y, \sigma_z)$ is the Pauli matrix of spin-1/2, and σ_0 is the identify matrix. $B_0(\mathbf{k})\sigma_0$ does not affect the band topology of $H(\mathbf{k})$ in the insulating phase; but topological states in the metallic phase disappear in the projection spectra where the two bands are inseparable. Topological properties of $H(\mathbf{k})$ are encoded in $\mathbf{B}(\mathbf{k})$, which may form closed surfaces in three-dimension. Any close surface wrapping the origin positively or negatively contributes to the Chern number. We find the coexistence of positive and negative wrappings, which creates the time-reversal symmetry breaking topological insulating phases that simultaneously holding the opposite chiral edge states. The Chern number is insufficient to characterize these novel band topologies, but the BCS distinguishes these topological insulating phases (Fig. 1).

The Chern number $C_\pm = (2\pi)^{-1} \iint_{\mathrm{BZ}} \mathrm{d}^2\mathbf{k} \cdot \mathbf{\Omega}_\pm(\mathbf{k})$ is the integral of Berry curvature $\mathbf{\Omega}_\pm(\mathbf{k}) = \nabla_\mathbf{k} \times \mathbf{A}_\pm(\mathbf{k})$ over the entire Brillouin zone (BZ), where $\mathbf{A}_\pm(\mathbf{k}) = -i\langle\psi_\pm(\mathbf{k})|\nabla_\mathbf{k}|\psi_\pm(\mathbf{k})\rangle$ is the Berry connection [1]. The subscript $+$ $(-)$ is for the upper (lower) band. The Bloch wave function is

$$|\psi_\pm(\mathbf{k})\rangle = \frac{1}{\sqrt{2h(\mathbf{k})[h(\mathbf{k}) \pm h_z(\mathbf{k})]}} \begin{pmatrix} h_z(\mathbf{k}) \pm h(\mathbf{k}) \\ h_x(\mathbf{k}) + ih_y(\mathbf{k}) \end{pmatrix}, \tag{1}$$

for the band energy $\varepsilon_\pm(\mathbf{k}) = B_0(\mathbf{k}) \pm [h_x^2(\mathbf{k}) + h_y^2(\mathbf{k}) + h_z^2(\mathbf{k})]^{1/2} = B_0(\mathbf{k}) \pm h(\mathbf{k})$. The Berry connection $\mathbf{A}_\pm(\mathbf{k})$ has the non-analytic points (BCSs) at

$$[h_x(\mathbf{k}), h_y(\mathbf{k}), h_z(\mathbf{k})] = [0, 0, \mp h(\mathbf{k})]. \tag{2}$$

The BCS on the band inversion surface $h_z(\mathbf{k}) = 0$ is the degenerate point $h(\mathbf{k}) = 0$ [64]. When the BCS moving across the band inversion surface, the band gap closes and reopens associated with the topological phase transition [2,65]. The charge of BCS $c_s = (2\pi)^{-1} \oint_{l_s} [h_y(\mathbf{k})dh_x(\mathbf{k}) - h_x(\mathbf{k})dh_y(\mathbf{k})]/[h_x^2(\mathbf{k}) + h_y^2(\mathbf{k})]$ is associated with the charge of degenerate point, being a positive charge $+1$ or a negative charge -1. The closed loop l_s in the BZ encloses only one BCS.

The singularities of $\mathbf{A}_+(\mathbf{k})$ and $\mathbf{A}_-(\mathbf{k})$ appear at $h_z(\mathbf{k}) = -h(\mathbf{k}) < 0$ and $h_z(\mathbf{k}) = +h(\mathbf{k}) > 0$, respectively. The regions $h_z(\mathbf{k}) < 0$ in the BZ are denoted as D_+ in yellow for the upper band and the regions $h_z(\mathbf{k}) > 0$ in the BZ are denoted as D_- in white for the lower band. The sum of all the singularity charges in the area D_+ (D_-) is the upper (lower) Chern number $C_+^{[m,n]} = m - n$ $(C_-^{[n,m]} = n - m)$ [66]. We use the upper band Chern number to describe the topological phase and remove the band index for conciseness. The superscripts in $C^{[m,n]}$ represent m positive and n negative BCSs, being the minimum numbers of singularities under any chosen gauge, is equal to the numbers of positive and negative wrappings in $\mathbf{B}(\mathbf{k})$. Figure 2(a) shows the BCSs in the BZ for the phase $C^{[1,1]}$. The red (cyan) cross in the yellow area indicates the singularity with positive (negative) charge $+1$ (-1) and predicts a clockwise (counterclockwise) propagating chiral edge state [Fig. 2(b)].

The Chern number is zero if the Berry connection is smooth. The presence of BCSs causes nontrivial topology. The BCSs originate from the degenerate points. The change on the total positive (negative) charge of BCSs before and after the topological phase transition is the total positive (negative) charge of degenerate points at the topological phase transition. The nonzero number of BCSs predicts the existence of gapless edge states. At the interface between two topological areas, the number of clockwise (counterclockwise) propagating edge states is equal to the difference between their total positive (negative) charges of BCSs. The BCSs present in the novel Chern insulators for $mn \neq 0$ and the conventional Chern insulators for $mn = 0$ (i.e., $C^{[m,0]}$ or $C^{[0,n]}$). By contrast, the two-dimensional Zak phase is valid when the entire BZ does not have any BCS in the phase $C^{[0,0]}$. The nonzero two-dimensional Zak phase predicts the existence of in-gap edge states [53,54]. These arguments are also valid for the multiband Chern insulators.

Topological phases $C^{[m,n]}$ and $C^{[m',n']}$ with different positive and/or negative charges have different band topologies, which lead to zeros in their wave function overlaps

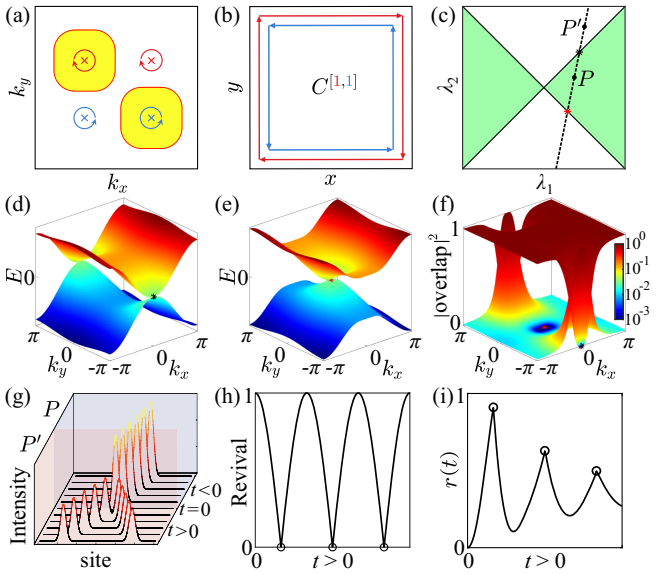

FIG. 2. Schematics of the edge state, band topology, and time boundary effect. (a) BCSs in the BZ. The red curves are the band inversion surface. (b) Coexistence of opposite chiral edge states. (c) Phase diagram in the parameter space λ_1-λ_2. The black solid lines indicate the topological phase transition. (d) [(e)] Energy bands at the black (red) star in (c). (f) Wave function overlaps between identical (different) Bloch bands for the system at the points P and P' are mainly in red (blue). (g) Equal time reflection and refraction for the initial state at a critical momentum. (h) Revival amplitude. (i) Rate function. In (g)–(i), the parameters before and after the time boundary are P and P'.

$\langle\psi'_{q'}(\mathbf{k})|\psi_q(\mathbf{k})\rangle$ (the subscripts q, q' are the band indices). The number of overlap zeros in the BZ is at least $|m-m'|+|n-n'|$, being the *minimum* number of degenerate points experienced in the topological phase transition for the band topology altering from $C^{[m,n]}$ to $C^{[m',n']}$ and vise versa. The overlap zeros present in any pair of wave function $|\psi_q(\mathbf{k})\rangle$ chosen from $C^{[m,n]}$ and wave function $|\psi'_{q'}(\mathbf{k})\rangle$ chosen from $C^{[m',n']}$; their existence is topologically protected. Figure 2(c) shows a phase diagram. The dashed straight line along the point P chosen from $C^{[m,n]}$ and the point P' chosen from $C^{[m',n']}$ crosses the solid lines at the black and red stars. Then, the wave functions at the points P and P' have zeros in their overlap $\langle\psi'_{q'}(\mathbf{k})|\psi_q(\mathbf{k})\rangle$ between identical (different) bands for $q=q'$ ($q\neq q'$), and the overlap zeros appear at the degenerate points for the system at the topological phase transition as marked by the black (red) star inside (outside) the points P and P' (see Supplemental Material B for the proof [63]), i.e., the overlap zeros imprint the band gap closing. Figure 2(d) [Fig. 2(e)] illustrates the energy bands at the black (red) star in Fig. 2(c), where the degenerate point is marked by the black (red) star. Figure 2(f) illustrates the overlaps between wave functions at the points P and P'; their zeros appear at these degenerate points.

The intriguing features present at the topological time boundary $t=0$ created via abruptly altering the system into a different topological phase. The revival amplitude $g(\mathbf{k},t)=\langle\Psi(0)|\Psi(t)\rangle$ between the initial state $|\Psi(0)\rangle=|\psi_-(\mathbf{k})\rangle$ before the time boundary and the evolution state $|\Psi(t)\rangle=e^{-itH'(\mathbf{k})}|\psi_-(\mathbf{k})\rangle$ driven by the Bloch Hamiltonian $H'(\mathbf{k})$ after the time boundary is

$$g(\mathbf{k},t)=\sum_{q'=\pm}|\langle\psi'_{q'}(\mathbf{k})|\psi_-(\mathbf{k})\rangle|^2e^{-it\varepsilon'_{q'}(\mathbf{k})}, \tag{3}$$

where the wave function $|\psi'_{q'}(\mathbf{k})\rangle$ of $H'(\mathbf{k})$ has the energy $\varepsilon'_{q'}(\mathbf{k})$. The wave function overlaps $|\langle\psi'_+(\mathbf{k})|\psi_-(\mathbf{k})\rangle|^2$ and $|\langle\psi'_-(\mathbf{k})|\psi_-(\mathbf{k})\rangle|^2$ predict the reflection and refraction at the time boundary, where the time-refracted (time-reflected) wave has the same (opposite) propagating direction with the initial wave. The wave momentum conserves before and after the time boundary and $\sum_{q'=\pm}|\langle\psi'_{q'}(\mathbf{k})|\psi_-(\mathbf{k})\rangle|^2=1$ [67–69].

Different band topologies before and after the time boundary ensure the existence of vanishing time reflection and refraction at different momenta $\mathbf{k}_1$ and $\mathbf{k}_2$. Consequently, a critical momentum $\mathbf{k}^\star=(k_x^\star,k_y^\star)$ associated with equal time reflection and refraction $|\langle\psi'_\pm(\mathbf{k}^\star)|\psi_-(\mathbf{k}^\star)\rangle|^2=1/2$ must exist between $\mathbf{k}_1$ and $\mathbf{k}_2$; and the number of critical momenta is at least the difference between the topological numbers before and after the time boundary $|m-m'|+|n-n'|$. Figure 2(g) illustrates the time reflection and refraction of an initial state at the critical momentum $k_c=k_y^\star$ (or $k_c=k_x^\star$) prepared in the one-dimensional projection system with $k_x=k_x^\star$ (or $k_y=k_y^\star$).

The revival amplitude for the initial state at the critical momentum periodically vanishes $g(\mathbf{k}^\star,t^\star)=e^{-itB'_0(\mathbf{k})}\cos[h'(\mathbf{k}^\star)t^\star]=0$ at the critical times [Fig. 2(h)]

$$t^\star=(M-1/2)\pi/h'(\mathbf{k}^\star), \tag{4}$$

where $M\in\mathbb{N}$ is a positive integer and the revival amplitude is nonanalytic. By contrast, the revival amplitude does not vanish for the initial state not at the critical momentum. The nonanalytic rate function [Fig. 2(i)] $r(t)=-(1/N)\ln\prod_{k_y}|g(k_x^\star,k_y,t)|^2$ at the critical times for the lattice size N is a dynamical analog of the nonanalytic free energy density at the critical temperature [70–72], where the revival amplitude is analogous to the partition function and the rate function is analogous to the free energy density. The existence of nonanalytic behavior in the time boundary effect is topologically protected.

Figure 3(a) illustrates an inversion symmetric square lattice with broken time-reversal symmetry [73–76]. The one-dimensional projection lattice after the Fourier transformation in the x direction is a generalized Su-Schrieffer-Heeger model with the long-range coupling [77], which

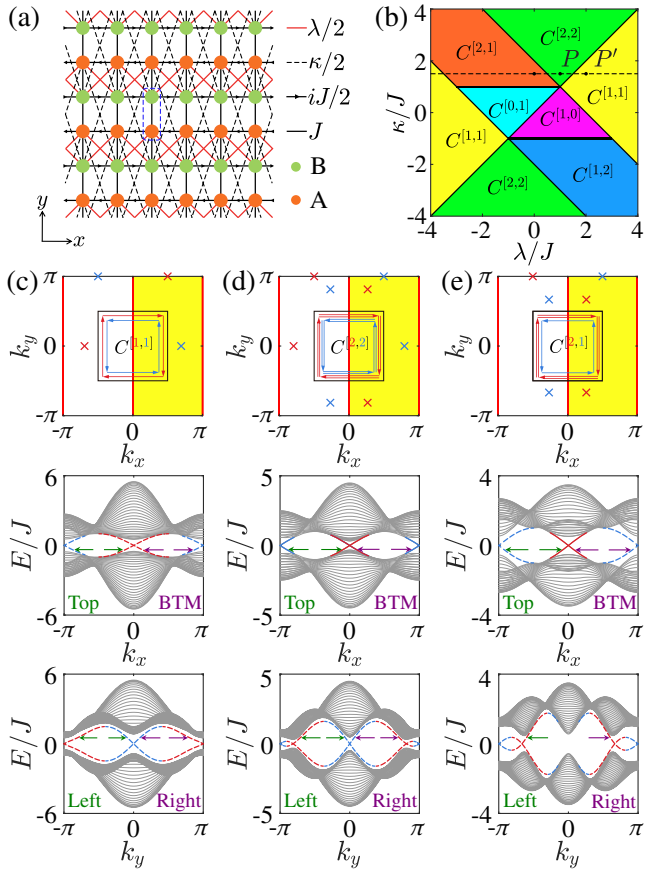

FIG. 3. (a) Square lattice. (b) Phase diagram. The distribution of BCSs, the schematic of edge states, and the projected band structures for the phases (c) $C^{[1,1]}$ at $(\lambda,\kappa)=(2J,3J/2)$, (d) $C^{[2,2]}$ at $(\lambda,\kappa)=(J,3J/2)$, (e) $C^{[2,1]}$ at $(\lambda,\kappa)=(0,3J/2)$. The dashed (solid) colored lines indicate one (twofold degenerate) edge state [83]. The abbreviation BTM stands for bottom.

becomes the nearest-neighbor coupling if the square lattice is rearranged into bilayer [45,60]; this model is equivalent to the coupled Su-Schrieffer-Heeger ladder [78], which is implemented in the coupled resonators [79,80]. The one-dimensional projection lattice after the Fourier transformation in the y direction is the Creutz ladder [81,82]. The effective magnetic field in the Bloch Hamiltonian after the Fourier transformations in both directions is $h_x(\mathbf{k})=J+(J+\lambda\cos k_x)\cos k_y+\kappa\cos k_x\cos(2k_y)$, $h_y(\mathbf{k})=(J+\lambda\cos k_x)\sin k_y+\kappa\cos k_x\sin(2k_y)$, $h_z(\mathbf{k})=-J\sin k_x$, and $B_0(\mathbf{k})=0$.

Figure 3(b) shows the phase diagram. The number of positive (negative) BCSs predicts the number of clockwise (counterclockwise) chiral edge states in red (cyan), counted from their crossings at the band gap closing degenerate points. The creation (annihilation) of edge states is associated with the creation (annihilation) of BCSs at the topological phase transition. Figures 3(c)–3(e) exhibit the BCSs and spectra of the novel topological phases $C^{[1,1]}$, $C^{[2,2]}$, and $C^{[2,1]}$. The opposite chiral edge states in

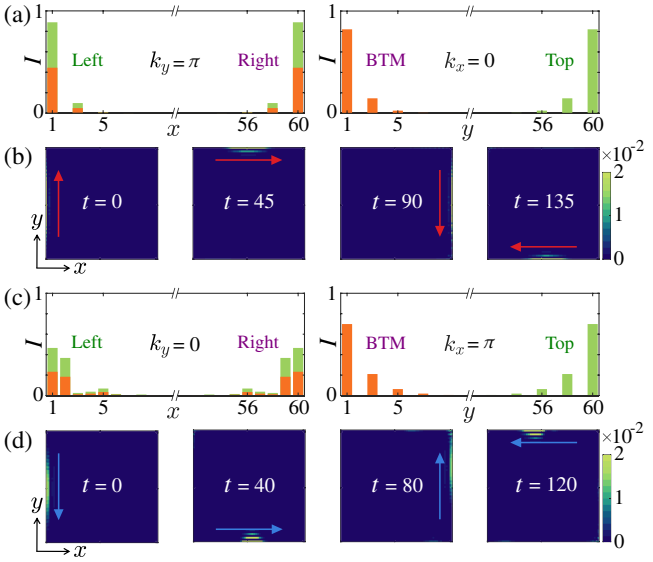

FIG. 4. The intensities of the (a) clockwise and (c) counterclockwise edge states in Fig. 3(c) at the marked momenta. The orange and green bars are for the sublattices A and B, respectively. The propagation of left edge state excitation centered at (b) $k_y=\pi$ and (d) $k_y=0$ in a 60×60 lattice.

the phase $C^{[1,1]}$ and their propagations are shown in Fig. 4 (see Supplemental Material C for the detail and robustness [63]). The propagations in opposite directions have different periods. In experiments, the realization of the phase $C^{[1,1]}$ at $\kappa=0$ only requires the next-nearest-neighbor coupling [41,84–86]. The long-range couplings enrich the novel topological phases $C^{[m,n]}$ with $mn\neq0$ in the photonic and acoustic metamaterials [77,87].

Topological overlap zeros present in the Bloch wave functions from any two different topological phases. For example, we consider the point P at $(\lambda,\kappa)=(J,3J/2)$ chosen from $C^{[2,2]}$ and the point P' at $(\lambda,\kappa)=(2J,3J/2)$ chosen from $C^{[1,1]}$. Both topological phases have a zero Chern number and differ from $C^{[0,0]}$ [88]. In the phase diagram Fig. 3(b), the straight dashed line along the points P and P' crosses three solid lines of topological phase transitions. At the cross inside the points P and P', the degenerate points are $(k_x,k_y)=(0,\pi)$ and (π,π). In Fig. 5(a), the overlap $|\langle\psi'_-(\mathbf{k})|\psi_-(\mathbf{k})\rangle|^2$ vanishes at these degenerate points as marked by the black stars. At the crosses outside the points P and P', the degenerate points are $(k_x,k_y)=(\pi,0)$ and $(0,0)$. In Fig. 5(a), the overlap $|\langle\psi'_+(\mathbf{k})|\psi_-(\mathbf{k})\rangle|^2$ vanishes at these degenerate points as marked by the red stars. In addition, two degenerate lines appear at $k_x=\pm\pi/2$ for $\lambda/J\to\pm\infty$, where $|\langle\psi'_+(\mathbf{k})|\psi_-(\mathbf{k})\rangle|^2=0$.

The vanishing revival amplitude in the time boundary effect witnesses the inequivalent band topologies before and after the time boundary (see Supplemental Material D for the experimental realization [63]). Figure 5(b) exhibits

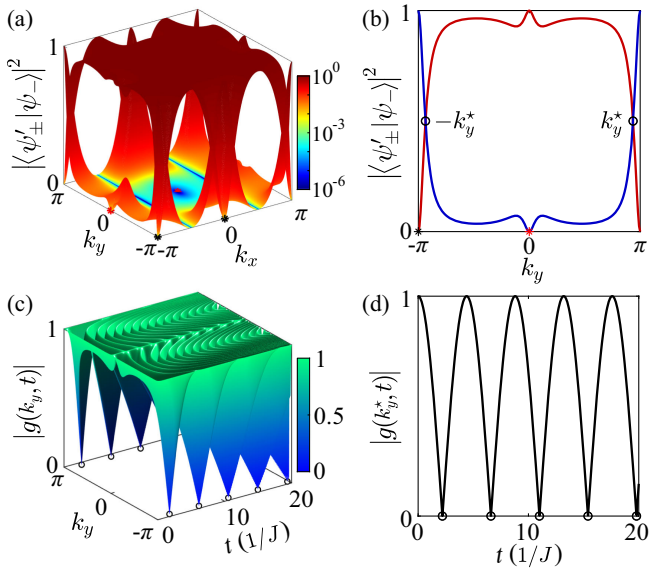

FIG. 5. (a) Overlap in the BZ. (b) Overlap at $k_x = \pi$. (c) Revival amplitude in (b) for the initial state $|\psi_-(\pi, k_y)\rangle$ before the time boundary chosen from $C^{[2,2]}$ [Fig. 3(d)] and the system after the time boundary chosen from $C^{[1,1]}$ [Fig. 3(c)]. (d) Revival amplitude in (c) at the critical momentum $k_y^\star$.

the reflection and refraction at the time boundary in the generalized Su-Schrieffer-Heeger model with $k_x = \pi$ for the initial state $|\psi_-(\pi, k_y)\rangle$, where the red curve is the time refraction $|\langle\psi'_-(\pi, k_y)|\psi_-(\pi, k_y)\rangle|^2$, the blue curve is the time reflection $|\langle\psi'_+(\pi, k_y)|\psi_-(\pi, k_y)\rangle|^2$, and $k_y^\star = 0.936\pi$ is the critical momentum. Figure 5(c) shows the revival amplitude $g(\pi, k_y, t)$, which periodically vanishes at the critical times $t^\star = 2.2/J, 6.6/J, 11.0/J, \cdots$ for $k_y = k_y^\star$ as indicated by the black hollow circles in Fig. 5(d). Similar behaviors exist in the time boundary effect performed in the Creutz ladder with $k_y = \pi$ for the initial state $|\psi_-(k_x^\star, \pi)\rangle$.

In summary, we proposed the novel band topologies, which enrich the kaleidoscopes of Chern insulators and gapless edge states. The coexistence of opposite chiral edge states opens a new door for the robust light transport [89]. We found that topological zeros present in the overlaps between Bloch wave functions from different topological phases at the degenerate points of topological phase transition and imprint the band gap closing. The overlap zeros correspond to the vanishing of time reflection or refraction [69] and ensure the existence of nonanalytic behavior in the time boundary effect as a witness of the different band topologies before and after the time boundary. The time boundaries create photonic time crystals [90], realize broadband frequency translation [91], and offer controllable light manipulation in synthetic dimension [92], our findings pave the way for exploring topology using the nonequilibrium dynamics of photons at the time boundary. It is interesting to further consider the photonic time boundary effect in non-Hermitian topological phases [93–100].

This work was supported by National Natural Science Foundation of China (Grants No. 12222504, No. 12305033, and No. 11975128).

*Corresponding author: jinliang@nankai.edu.cn

[1] L. Lu, J. D. Joannopoulos, and M. Soljačić, Topological photonics, Nat. Photonics **8**, 821 (2014); Topological states in photonic systems, Nat. Phys. **12**, 626 (2016).
[2] A. B. Khanikaev and G. Shvets, Two-dimensional topological photonics, Nat. Photonics **11**, 763 (2017).
[3] Y. Wu, C. Li, X. Hu, Y. Ao, Y. Zhao, and Q. Gong, Applications of topological photonics in integrated photonic devices, Adv. Opt. Mater. **5**, 1700357 (2017).
[4] B.-Y. Xie, H.-F. Wang, X.-Y. Zhu, M.-H. Lu, Z. D. Wang, and Y.-F. Chen, Photonics meets topology, Opt. Express **26**, 24531 (2018).
[5] T. Ozawa, H. M. Price, A. Amo, N. Goldman, M. Hafezi, L. Lu, M. C. Rechtsman, D. Schuster, J. Simon, O. Zilberberg, and I. Carusotto, Topological photonics, Rev. Mod. Phys. **91**, 015006 (2019).
[6] G. Ma, M. Xiao, and C. T. Chan, Topological phases in acoustic and mechanical systems, Nat. Rev. Phys. **1**, 281 (2019).
[7] D. Leykam and L. Yuan, Topological phases in ring resonators: Recent progress and future prospects, Nanophotonics **9**, 4473 (2020).
[8] Y. Ota, K. Takata, T. Ozawa, A. Amo, Z. Jia, B. Kante, M. Notomi, Y. Arakawa, and S. Iwamoto, Active topological photonics, Nanophotonics **9**, 547 (2020).
[9] M. Kim, Z. Jacob, and J. Rho, Recent advances in 2D, 3D and higher-order topological photonics, Light Sci. Appl. **9**, 130 (2020).
[10] Z. Chen and M. Segev, Highlighting photonics: Looking into the next decade, eLight **1**, 2 (2021).
[11] G. J. Tang, X. T. He, F. L. Shi, J. W. Liu, X. D. Chen, and J. W. Dong, Topological photonic crystals: Physics, designs, and applications, Laser Photonics Rev. **16**, 2100300 (2022).
[12] H. Price, Y. Chong, A. Khanikaev, H. Schomerus, L. J. Maczewsky, M. Kremer, M. Heinrich, A. Szameit, O. Zilberberg, Y. Yang, B. Zhang, A. Alù, R. Thomale, I. Carusotto, P. St-Jean, A. Amo, A. Dutt, L. Yuan, S. Fan, X. Yin, C. Peng, T. Ozawa, and A. Blanco-Redondo, Roadmap on topological photonics, J. Phys. Photonics **4**, 032501 (2022).
[13] Z.-K. Lin, Q. Wang, Y. Liu, H. Xue, B. Zhang, Y. Chong, and J.-H. Jiang, Topological phenomena at defects in acoustic, photonic and solid-state lattices, Nat. Rev. Phys. **5**, 483 (2023).
[14] M. Z. Hasan and C. L. Kane, Colloquium: Topological insulators, Rev. Mod. Phys. **82**, 3045 (2010); X.-L. Qi and S.-C. Zhang, Topological insulators and superconductors, Rev. Mod. Phys. **83**, 1057 (2011); E. J. Bergholtz, J. C. Budich, and F. K. Kunst, Exceptional topology of

non-Hermitian systems, Rev. Mod. Phys. **93**, 015005 (2021).
[15] Y. Ashida, Z. Gong, and M. Ueda, Non-Hermitian physics, Adv. Phys. **69**, 249 (2020).
[16] K. Ding, C. Fang, and G. Ma, Non-Hermitian topology and exceptional-point geometries, Nat. Rev. Phys. **4**, 745 (2022).
[17] R. Lin, T. Tai, L. Li, and C. H. Lee, Topological non-Hermitian skin effect, Front. Phys. **18**, 53605 (2023).
[18] S. Mittal, S. Ganeshan, J. Fan, A. Vaezi, and M. Hafezi, Measurement of topological invariants in a 2D photonic system, Nat. Photonics **10**, 180 (2016).
[19] F. Cardano, A. D'Errico1, A. Dauphin, M. Maffei, B. Piccirillo, C. de Lisio, G. De Filippis, V. Cataudella, E. Santamato, L. Marrucci, M. Lewenstein, and P. Massignan, Detection of Zak phases and topological invariants in a chiral quantum walk of twisted photons, Nat. Commun. **8**, 15516 (2017).
[20] O. Zilberberg, S. Huang, J. Guglielmon, M. Wang, K. P. Chen, Y. E. Kraus, and M. C. Rechtsman, Photonic topological boundary pumping as a probe of 4D quantum Hall physics, Nature (London) **553**, 59 (2018).
[21] D. Leykam and D. A. Smirnova, Probing bulk topological invariants using leaky photonic lattices, Nat. Phys. **17**, 632 (2021).
[22] L.-C. Wang, Y. Chen, M. Gong, F. Yu, Q.-D. Chen, Z.-N. Tian, X.-F. Ren, and H.-B. Sun, Edge state, localization length, and critical exponent from survival probability in topological waveguides, Phys. Rev. Lett. **129**, 173601 (2022).
[23] G. Li, L. Wang, R. Ye, Y. Zheng, D.-W. Wang, X.-J. Liu, A. Dutt, L. Yuan, and X. Chen, Direct extraction of topological Zak phase with the synthetic dimension, Light Sci. Appl. **12**, 81 (2023).
[24] F. D. M. Haldane and S. Raghu, Possible realization of directional optical waveguides in photonic crystals with broken time-reversal symmetry, Phys. Rev. Lett. **100**, 013904 (2008).
[25] Z. Wang, Y. Chong, J. D. Joannopoulos, and M. Soljačić, Observation of unidirectional backscattering-immune topological electromagnetic states, Nature (London) **461**, 772 (2009).
[26] K. Fang, Z. Yu, and S. Fan, Realizing effective magnetic field for photons by controlling the phase of dynamic modulation, Nat. Photonics **6**, 782 (2012).
[27] M. C. Rechtsman, J. M. Zeuner, Y. Plotnik, Y. Lumer, D. Podolsky, F. Dreisow, S. Nolte, M. Segev, and A. Szameit, Photonic Floquet topological insulators, Nature (London) **496**, 196 (2013).
[28] Z. Yang, F. Gao, X. Shi, X. Lin, Z. Gao, Y. Chong, and B. Zhang, Topological acoustics, Phys. Rev. Lett. **114**, 114301 (2015).
[29] S. A. Skirlo, L. Lu, Y. Igarashi, Q. Yan, J. Joannopoulos, and M. Soljačić, Experimental observation of large Chern numbers in photonic crystals, Phys. Rev. Lett. **115**, 253901 (2015).
[30] K. Chen and A. B. Khanikaev, Non-Hermitian $C_{NH} = 2$ Chern insulator protected by generalized rotational symmetry, Phys. Rev. B **105**, L081112 (2022).
[31] Z. Wang, Y. Biao, X.-T. Zeng, X. Chen, X.-L. Sheng, S. A. Yang, and R. Yu, Realization in circuits of a Chern state with an arbitrary Chern number, Phys. Rev. B **107**, L201101 (2023).
[32] M. Hafezi, E. A. Demler, M. D. Lukin, and J. M. Taylor, Robust optical delay lines with topological protection, Nat. Phys. **7**, 907 (2011).
[33] A. B. Khanikaev, S. H. Mousavi, W.-K. Tse, M. Kargarian, A. H. MacDonald, and G. Shvets, Photonic topological insulators, Nat. Mater. **12**, 233 (2013).
[34] X. Yin, Z. Ye, J. Rho, Y. Wang, and X. Zhang, Photonic spin Hall effect at metasurfaces, Science **339**, 1405 (2013).
[35] W.-J. Chen, S.-J. Jiang, X.-D. Chen, B. Zhu, L. Zhou, J.-W. Dong, and C. T. Chan, Experimental realization of photonic topological insulator in a uniaxial metacrystal waveguide, Nat. Commun. **5**, 5782 (2014).
[36] K. Y. Bliokh, D. Smirnova, and F. Nori, Quantum spin Hall effect of light, Science **348**, 1448 (2015).
[37] L.-H. Wu and X. Hu, Scheme for achieving a topological photonic crystal by using dielectric material, Phys. Rev. Lett. **114**, 223901 (2015).
[38] C. He, X.-C. Sun, X.-P. Liu, M.-H. Lu, Y. Chen, L. Feng, and Y.-F. Chen, Photonic topological insulator with broken time-reversal symmetry, Proc. Natl. Acad. Sci. U.S.A. **113**, 4924 (2016).
[39] L. J. Maczewsky, J. M. Zeuner, S. Nolte, and A. Szameit, Observation of photonic anomalous Floquet topological insulators, Nat. Commun. **8**, 13756 (2017).
[40] S. Mukherjee, A. Spracklen, M. Valiente, E. Andersson, P. Öhberg, N. Goldman, and R. R. Thomson, Experimental observation of anomalous topological edge modes in a slowly driven photonic lattice, Nat. Commun. **8**, 13918 (2017).
[41] D. Leykam, S. Mittal, M. Hafezi, and Y. D. Chong, Reconfigurable topological phases in next-nearest-neighbor coupled resonator lattices, Phys. Rev. Lett. **121**, 023901 (2018).
[42] Y. Yang, Y. F. Xu, T. Xu, H. X. Wang, J. H. Jiang, X. Hu, and Z. H. Hang, Visualization of unidirectional optical waveguide using topological photonic crystals made of dielectric material, Phys. Rev. Lett. **120**, 217401 (2018).
[43] S. Mittal, V. V. Orre, D. Leykam, Y. D. Chong, and M. Hafezi, Photonic anomalous quantum Hall effect, Phys. Rev. Lett. **123**, 043201 (2019).
[44] J.-W. Dong, X.-D. Chen, H. Zhu, Y. Wang, and X. Zhang, Valley photonic crystals for control of spin and topology, Nat. Mater. **16**, 298 (2017).
[45] J. Lu, C. Qiu, W. Deng, X. Huang, F. Li, F. Zhang, S. Chen, and Z. Liu, Valley topological phases in bilayer sonic crystals, Phys. Rev. Lett. **120**, 116802 (2018).
[46] F. Gao, H. Xue, Z. Yang, K. Lai, Y. Yu, X. Lin, Y. Chong, G. Shvets, and B. Zhang, Topologically protected refraction of robust kink states in valley photonic crystals, Nat. Phys. **14**, 140 (2018).
[47] Y. Kang, X. Ni, X. Cheng, A. B. Khanikaev, and A. Z. Genack, Pseudo-spin-valley coupled edge states in a photonic topological insulator, Nat. Commun. **9**, 3029 (2018).

[48] J. Noh, S. Huang, K. P. Chen, and M. C. Rechtsman, Observation of photonic topological valley Hall edge states, Phys. Rev. Lett. **120**, 063902 (2018).
[49] X.-D. Chen, F.-L. Shi, H. Liu, J.-C. Lu, W.-M. Deng, J.-Y. Dai, Q. Cheng, and J.-W. Dong, Tunable electromagnetic flow control in valley photonic crystal waveguides, Phys. Rev. Appl. **10**, 044002 (2018).
[50] L. Zhang, Y. Yang, M. He, H.-X. Wang, Z. Yang, E. Li, F. Gao, B. Zhang, R. Singh, J.-H. Jiang, and H. Chen, Valley kink states and topological channel intersections in substrate-integrated photonic circuitry, Laser Photonics Rev. **13**, 1900159 (2019).
[51] H. Yang, J. Xu, Z. Xiong, X. Lu, R. Y. Zhang, H. Li, Y. Chen, and S. Zhang, Optically reconfigurable spin-valley Hall effect of light in coupled nonlinear ring resonator lattice, Phys. Rev. Lett. **127**, 043904 (2020).
[52] H. Zhong, S. Xia, Y. Zhang, Y. Li, D. Song, C. Liu, and Z. Chen, Nonlinear topological valley Hall edge states arising from type-II Dirac cones, Adv. Photonics **3**, 056001 (2021).
[53] F. Liu and K. Wakabayashi, Novel topological phase with a zero Berry curvature, Phys. Rev. Lett. **118**, 076803 (2017).
[54] W. A. Benalcazar, B. A. Bernevig, and T. L. Hughes, Quantized electric multipole insulators, Science **357**, 61 (2017).
[55] X.-D. Chen, W.-M. Deng, F.-L. Shi, F.-L. Zhao, M. Chen, and J.-W. Dong, Direct observation of corner states in second-order topological photonic crystal slabs, Phys. Rev. Lett. **122**, 233902 (2019).
[56] B.-Y. Xie, G.-X. Su, H.-F. Wang, H. Su, X.-P. Shen, P. Zhan, M.-H. Lu, Z.-L. Wang, and Y.-F. Chen, Visualization of higher-order topological insulating phases in two-dimensional dielectric photonic crystals, Phys. Rev. Lett. **122**, 233903 (2019).
[57] S. Mittal, V. V. Orre, G. Zhu, M. A. Gorlach, A. Poddubny, and M. Hafezi, Photonic quadrupole topological phases, Nat. Photonics **13**, 692 (2019).
[58] L. He, Z. Addison, E. J. Mele, and B. Zhen, Quadrupole topological photonic crystals, Nat. Commun. **11**, 3119 (2020).
[59] M. S. Kirsch, Y. Zhang, M. Kremer, L. J. Maczewsky, S. K. Ivanov, Y. V. Kartashov, L. Torner, D. Bauer, A. Szameit, and M. Heinrich, Nonlinear second-order photonic topological insulators, Nat. Phys. **17**, 995 (2021).
[60] Y. Yang, J. Lu, M. Yan, X. Huang, W. Deng, and Z. Liu, Hybrid-order topological insulators in a phononic crystal, Phys. Rev. Lett. **126**, 156801 (2021).
[61] J. Schulz, J. Noh, W. A. Benalcazar, G. Bahl, and G. von Freymann, Photonic quadrupole topological insulator using orbital-induced synthetic flux, Nat. Commun. **13**, 6597 (2022).
[62] G. Xu, X. Zhou, S. Yang, J. Wu, and C.-W. Qiu, Observation of bulk quadrupole in topological heat transport, Nat. Commun. **14**, 3252 (2023).
[63] See Supplemental Material at http://link.aps.org/supplemental/10.1103/PhysRevLett.132.083801 for the examples of different two-dimensional topological phases, the proof of overlap zero of Bloch wave function, the details of the square lattice model, including the Berry connection singularity, the topological phase transition, the topological edge states, the robust propagation, and the experimental realization.
[64] L. Zhang, L. Zhang, S. Niu, and X.-J. Liu, Dynamical classification of topological quantum phases, Sci. Bull. **63**, 1385 (2018).
[65] Y. Ao, X. Hu, Y. You, C. Lu, Y. Fu, X. Wang, and Q. Gong, Topological phase transition in the non-Hermitian coupled resonator array, Phys. Rev. Lett. **125**, 013902 (2020).
[66] The numbers of removable BCSs in the BZ are excluded in counting the BCSs. The total numbers of BCSs for the upper and lower bands can be different under an improper gauge, but the minimum numbers of positive and negative BCSs for the upper and lower bands m, n are always interchanged. The extra BCSs, being gauge dependent, are removable under a proper gauge transformation. Notably, the proper gauge associated with the minimum number of BCSs is not unique.
[67] B. W. Plansinis, W. R. Donaldson, and G. P. Agrawal, What is the temporal analog of reflection and refraction of optical beams?, Phys. Rev. Lett. **115**, 183901 (2015).
[68] O. Y. Long, K. Wang, A. Dutt, and S. Fan, Time reflection and refraction in synthetic frequency dimension, Phys. Rev. Res. **5**, L012046 (2023).
[69] Z. Dong, H. Li, T. Wan, Q. Liang, Z. Yang, and B. Yan, Quantum time reflection and refraction of ultracold atoms, Nat. Photonics **18**, 68 (2024).
[70] Z. Huang and A. V. Balatsky, Dynamical quantum phase transitions: Role of topological nodes in wave function overlaps, Phys. Rev. Lett. **117**, 086802 (2016).
[71] K. Wang, X. Qiu, L. Xiao, X. Zhan, Z. Bian, W. Yi, and P. Xue, Simulating dynamic quantum phase transitions in photonic quantum walks, Phys. Rev. Lett. **122**, 020501 (2019).
[72] H. Hu and E. Zhao, Topological invariants for quantum quench dynamics from unitary evolution, Phys. Rev. Lett. **124**, 160402 (2020).
[73] M. Hafezi, S. Mittal, J. Fan, A. Migdall, and J. M. Taylor, Imaging topological edge states in silicon photonics, Nat. Photonics **7**, 1001 (2013).
[74] F. Gao, Z. Gao, X. Shi, Z. Yang, X. Lin, H. Xu, J. D. Joannopoulos, M. Soljačić, H. Chen, L. Lu, Y. Chong, and B. Zhang, Probing topological protection using a designer surface plasmon structure, Nat. Commun. **7**, 11619 (2016).
[75] S. Afzal, T. J. Zimmerling, Y. Ren, D. Perron, and V. Van, Realization of anomalous Floquet insulators in strongly coupled nanophotonic lattices, Phys. Rev. Lett. **124**, 253601 (2020).
[76] D. Zou, T. Chen, W. He, J. Bao, C. H. Lee, H. Sun, and X. Zhang, Observation of hybrid higher-order skin-topological effect in non-Hermitian topolectrical circuits, Nat. Commun. **12**, 7201 (2021).
[77] H. Liu, X. Huang, M. Yan, J. Lu, W. Deng, and Z. Liu, Acoustic topological metamaterials of large winding number, Phys. Rev. Appl. **19**, 054028 (2023).
[78] Z. Guo, J. Jiang, H. Jiang, J. Ren, and H. Chen, Observation of topological bound states in a double Su-Schrieffer-Heeger chain composed of split ring resonators, Phys. Rev. Res. **3**, 013122 (2021).

[79] G. Q. Liang and Y. D. Chong, Optical resonator analog of a two-dimensional topological insulator, Phys. Rev. Lett. **110**, 203904 (2013).
[80] H. C. Wu, X. M. Yang, L. Jin, and Z. Song, Untying links through anti-parity-time-symmetric coupling, Phys. Rev. B **102**, 161101(R) (2020).
[81] H. Cai, J. Liu, J. Wu, Y. He, S.-Y. Zhu, J.-X. Zhang, and D.-W. Wang, Experimental observation of momentum-space chiral edge currents in room-temperature atoms, Phys. Rev. Lett. **122**, 023601 (2019).
[82] L. Jin and Z. Song, Bulk-boundary correspondence in a non-Hermitian system in one dimension with chiral inversion symmetry, Phys. Rev. B **99**, 081103(R) (2019).
[83] The edge states are distinguishable from three aspects: (i) the chirality of propagation direction (clockwise or counterclockwise circulating), (ii) the degree of degeneracy (single one or twofold), (iii) the location position (on the top or bottom boundary for the open boundary condition in the y direction; on the left or right boundary for the open boundary condition in the x direction). In the spectrum under periodic boundary condition in the x direction and open boundary condition in the y direction, the red (cyan) edge states localized on the top or bottom boundary has a positive or negative (negative or positive) velocity. In the spectrum under open boundary condition in the x direction and periodic boundary condition in the y direction, the red (cyan) edge states localized on the left or right boundary have a positive or negative (negative or positive) velocity. Thus, the red (cyan) edge mode excitation clockwise (counterclockwise) propagates along the boundaries as indicated by the red (cyan) arrows.
[84] M. Li, D. Zhirihin, M. Gorlach, X. Ni, D. Filonov, A. Slobozhanyuk, A. Alù, and A. B. Khanikaev, Higher-order topological states in photonic kagome crystals with long-range interactions, Nat. Photonics **14**, 89 (2020).
[85] Y. Li, C. Liang, C. Wang, C. Lu, and Y.-C. Liu, Gain-loss-induced hybrid skin-topological effect, Phys. Rev. Lett. **128**, 223903 (2022).
[86] L. Xie, L. Jin, and Z. Song, Antihelical edge states in two-dimensional photonic topological metals, Sci. Bull. **68**, 255 (2023).
[87] Z. Wang, X. Wang, Z. Hu, D. Bongiovanni, D. Jukić, L. Tang, D. Song, R. Morandotti, Z. Chen, and H. Buljan, Sub-symmetry-protected topological states, Nat. Phys. **19**, 992 (2023).
[88] H. C. Wu, L. Jin, and Z. Song, Nontrivial topological phase with a zero Chern number, Phys. Rev. B **102**, 035145 (2020).
[89] B.-C. Xu, B.-Y. Xie, L.-H. Xu, M. Deng, W. Chen, H. Wei, F. Dong, J. Wang, C.-W. Qiu, S. Zhang, and L. Chen, Topological Landau-Zener nanophotonic circuits, Adv. Photonics **5**, 036005 (2023).
[90] E. Lustig, Y. Sharabi, and M. Segev, Topological aspects of photonic time crystals, Optica **5**, 1390 (2018).
[91] H. Moussa, G. Xu, S. Yin, E. Galiffi, Y. Ra'di, and A. Alù, Observation of temporal reflection and broadband frequency translation at photonic time interfaces, Nat. Phys. **19**, 863 (2023).
[92] H. Ye, C. Qin, S. Wang, L. Zhao, W. Liu, B. Wang, S. Longhi, and P. Lu, Reconfigurable refraction manipulation at synthetic temporal interfaces with scalar and vector gauge potentials, Proc. Natl. Acad. Sci. U.S.A. **120**, e2300860120 (2023).
[93] S. Malzard, C. Poli, and H. Schomerus, Topologically protected defect states in open photonic systems with non-Hermitian charge-conjugation and parity-time symmetry, Phys. Rev. Lett. **115**, 200402 (2015).
[94] L. Jin and Z. Song, Incident direction independent wave propagation and unidirectional lasing, Phys. Rev. Lett. **121**, 073901 (2018).
[95] H. Zhao, X. Qiao, T. Wu, B. Midya, S. Longhi, and L. Feng, Non-Hermitian topological light steering, Science **365**, 1163 (2019).
[96] S. Weidemann, M. Kremer, T. Helbig, T. Hofmann, A. Stegmaier, M. Greiter, R. Thomale, and A. Szameit, Topological funneling of light, Science **368**, 311 (2020).
[97] L. Xiao, T. Deng, K. Wang, G. Zhu, Z. Wang, W. Yi, and P. Xue, Non-Hermitian bulk-boundary correspondence in quantum dynamics, Nat. Phys. **16**, 761 (2020).
[98] L.-L. Wan and X.-Y. Lü, Quantum-squeezing-induced point-gap topology and skin effect, Phys. Rev. Lett. **130**, 203605 (2023).
[99] Y. Ke, J. Huang, W. Liu, Y. Kivshar, and C. Lee, Topological inverse band theory in waveguide quantum electrodynamics, Phys. Rev. Lett. **131**, 103604 (2023).
[100] T. Dai, Y. Ao, J. Mao, Y. Yang, Y. Zheng, C. Zhai, Y. Li, J. Yuan, B. Tang, Z. Li, J. Luo, W. Wang, X. Hu, Q. Gong, and J. Wang, Non-Hermitian topological phase transitions controlled by nonlinearity, Nat. Phys. **20**, 101 (2024).